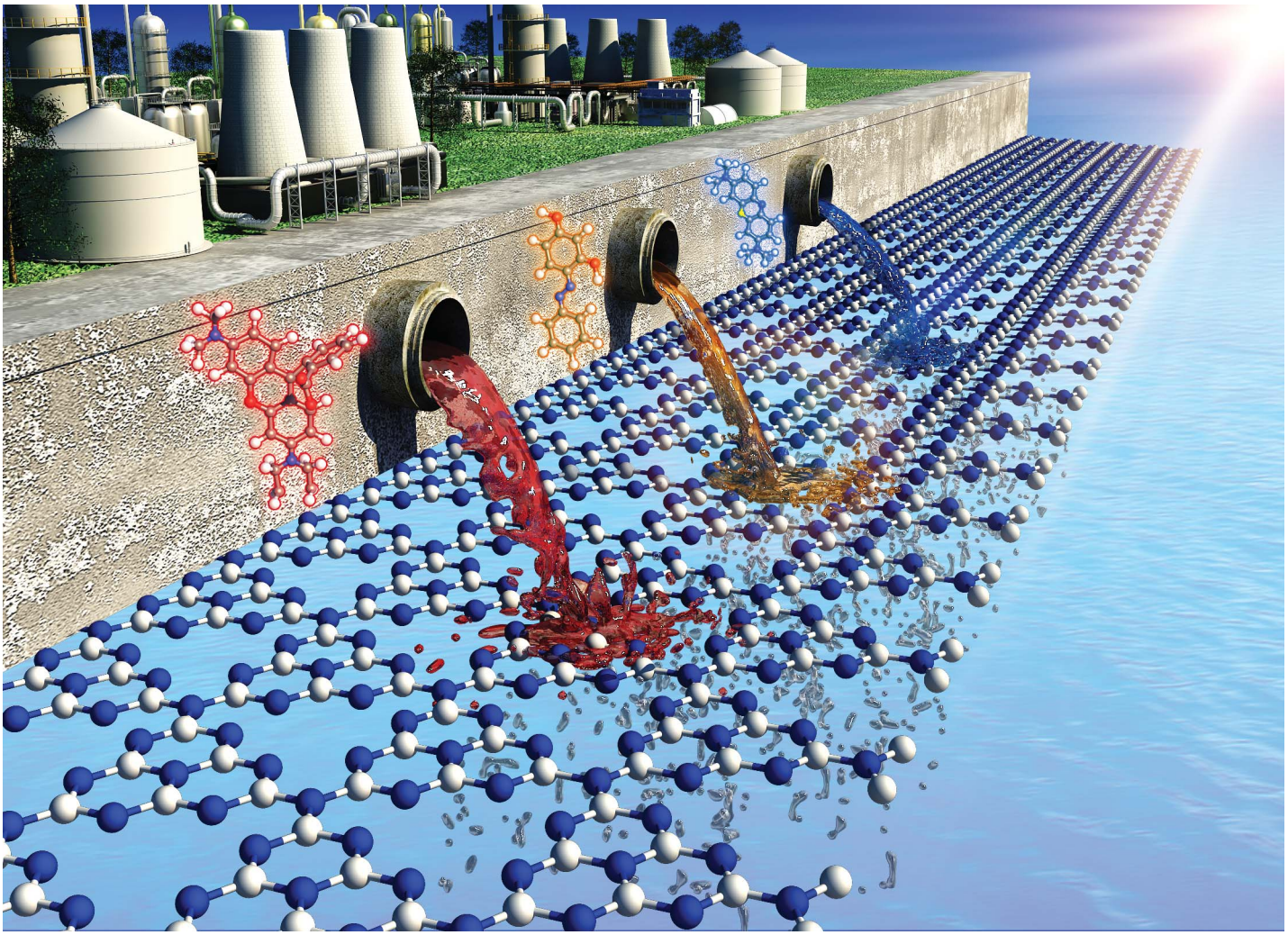

Showcasing research from the University of Manchester.

Self-catalytic membrane photo-reactor made of carbon nitride nanosheets

A novel membrane photo-reactor (MPR) was made of graphitic carbon nitride (g-C_3N_4) nanosheets. The g-C_3N_4 MPR is used as both separation layer and catalyst for high efficient photo-oxidation of organic dyes.

As featured in:

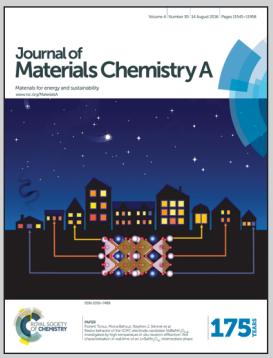

See Kai-Ge Zhou, Cinzia Casiraghi *et al.*, *J. Mater. Chem. A*, 2016, **4**, 11666.

ROYAL SOCIETY OF CHEMISTRY

www.rsc.org/MaterialsA

Registered charity number: 207890

Journal of Materials Chemistry A

PAPER

View Article Online
View Journal | View Issue

Cite this: J. Mater. Chem. A, 2016, 4, 11666

Self-catalytic membrane photo-reactor made of carbon nitride nanosheets†

Kai-Ge Zhou,*[a] Daryl McManus,[a] Eric Prestat,[b] Xing Zhong,[c] Yuyoung Shin,[a] Hao-Li Zhang,[d] Sarah J. Haigh[b] and Cinzia Casiraghi*[a]

Received 11th November 2015
Accepted 28th March 2016

DOI: 10.1039/c5ta09152g

www.rsc.org/MaterialsA

Solar-driven photo-oxidation is a very attractive and efficient technique for chemical conversion of organic dyes in water into non-hazardous compounds, but it requires a catalyst in order to overcome the barrier of oxidation degradation. In this study we use a membrane photo-reactor (MPR) made of nanosheets of graphitic carbon nitride (g-C_3N_4), assembled by vacuum filtration. The membrane was characterized by X-Ray Diffraction (XRD), Nuclear Magnetic Resonance (NMR), electron microscopy and IR spectroscopy. Photo-degradation studies show that the membranes are very efficient in the degradation of Sudan orange G, rhodamine 110 and methylene blue. As the catalyst is a porous laminate, the reactant can flow through the pores of the membrane. Because the space between g-C_3N_4 nanosheets is comparable to the size of the dyes, the probability of the reactants to be close to the catalyst is enhanced, making the reaction very efficient.

Introduction

The textile industry is the main source of organic pollution worldwide.[1–3] Many of the dyes used have complex structure and recalcitrant nature. They exhibit great biotoxicity and possible mutagenic and carcinogenic effects. Therefore, an efficient and low-cost technique for chemical conversion of the dyes into non-hazardous compounds is desirable. Solar-driven photo-oxidation is a very attractive technique, but requires a catalyst in order to overcome the barrier of oxidation degradation. Amongst all catalysts, TiO_2 nanoparticles are the best materials for photo-catalytic degradation of organic pollutants because of their high efficiency, availability, low cost, non-toxicity and chemical stability.[4] However, TiO_2 only absorbs UV light,[5–7] so its efficiency is very low when used for sunlight-driven photo-catalytic reactions. Various attempts have been made to modify TiO_2, either by changing its band structure or by combining it with an antenna for light absorption and transfer enhancement.[8–11] However, there are still issues on limited efficiency, reproducibility, controllability, and thermal stability of TiO_2 based catalysts.

Carbon nanostructures have been widely studied as catalysts for photo-oxidation reactions.[12,13] In particular, the family of carbon nitrides (C_3N_4)[14,15] offers a valid alternative to modified TiO_2. Graphitic-C_3N_4 (g-C_3N_4), which is the most stable form at room temperature, has been shown to be an efficient photo-catalyst for many reactions under visible light, from water splitting to oxidization of alkanes and olefins.[16–28] This ability has been attributed to its medium-band gap (~2.7 eV) and to its HOMO and LUMO levels, which encompass the oxidation and reduction potential of water.[16,29] Further improvement of the catalytic activity of g-C_3N_4 can be obtained by functionalization, similar to TiO_2.[16] An alternative approach consists of enhancing the interaction between the active site and the dye by increasing the surface area of the catalyst. Therefore, nanocasting and templating approaches have been used to produce mesoporous-C_3N_4 (mpg-C_3N_4).[30–32] Recently, a simple, low cost and controllable method to increase the catalytic efficiency of g-C_3N_4, based on the use of 2-Dimensional (2D) crystals, has been presented.[33–40] 2D crystals are a new class of stable, highly processable materials that feature distinctive properties compared to their 3D counterparts. Graphitic carbon nitride is a 2D covalent organic framework characterized by a three-folded symmetric arrangement of tris-*s*-triazine connected by tertiary amine in-plane (g-C_3N_4 bulk in Fig. 1a). In bulk g-C_3N_4, most of the catalytic sites are not directly available as they are inaccessible. Since bulk g-C_3N_4 is a layered material, the simplest way to maximize the exposure of the catalytic sites to the organic pollutant is to exfoliate the material into few and single-layer g-C_3N_4.[34,36,41] Bulk g-C_3N_4 can be efficiently exfoliated by using liquid-phase exfoliation (LPE) in IPA/water,[40,42,43] as shown in Fig. 1a.

[a]School of Chemistry, University of Manchester, Oxford Road, Manchester, M13 9PL, UK. E-mail: cinzia.casiraghi@manchester.ac.uk; zhkg7120@163.com
[b]School of Materials University of Manchester, Oxford Road, Manchester, M13 9PL, UK
[c]College of Chemical Engineering and Materials Science, Zhejiang University of Technology, Hangzhou 310014, P. R. China
[d]State Key Laboratory of Applied Organic Chemistry, Lanzhou University, Lanzhou 730000, P. R. China

† Electronic supplementary information (ESI) available: Preparation details, AFM, solid NMR, TEM, SEM and IR spectroscopy; photo-degradation studies using different reactors and control experiments. See DOI: 10.1039/c5ta09152g

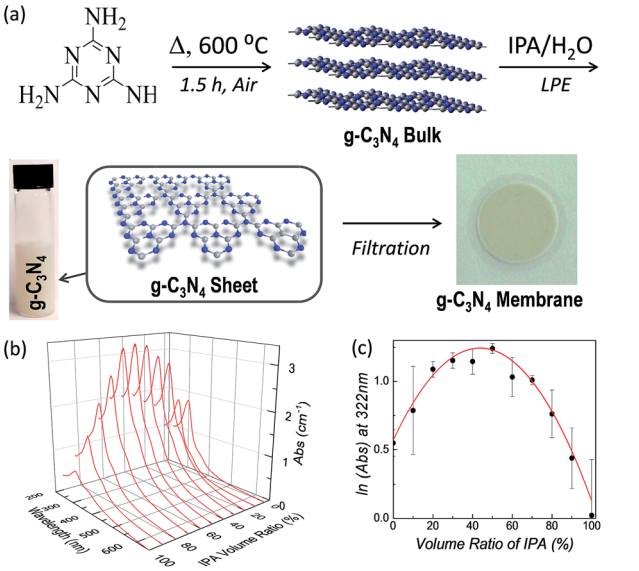

Fig. 1 (a) Schematic of the synthesis of g-C_3N_4 bulk and its liquid phase exfoliation in mixed solvents: the bulk graphitic carbon nitride is prepared by thermal annealing of melamine, followed by liquid-phase exfoliation in IPA/water. Membranes are obtained by using vacuum filtration. (b) Typical UV-Vis spectra of dispersed g-C_3N_4 in IPA/H_2O mixtures (diluted 10 times). (c) Concentration of dispersed g-C_3N_4 as a function of the solvent ratio. The red line is the fit obtained by using eqn (1) (see main text).

Results and discussion

By using the LPE theory for mixed solvents[43] (full details in the Section 1.1 of the ESI†) we found that the natural logarithm of the concentration of the dispersed material (C) is a quadratic function of the IPA volume ratio φ:

$$\ln C = A + B\varphi + C\varphi^2 \quad (1)$$

where A, B, C are three constants. By using different IPA volume ratios and measuring the concentration by UV-Vis spectroscopy, Fig. 1a and c, we found that the maximum concentration (~0.7 mg mL^{-1}) is obtained at 44% volume ratio, giving a yield of 35%, in agreement with results obtained for other 2D crystals.[44] Note that our result is in strong disagreement with ref. 40 which claims a yield of 90%, which has never been reported for LPE of 2D crystals.

LPE g-C_3N_4 nanosheets, used in traditional slurry-batch photo-reactors, show improved catalytic efficiency for photo-degradation of several dyes (Section S3 in ESI†) due to the larger surface area and possibly due to possessing different optical and electrical properties compared to bulk g-C_3N_4.[40,45] However, conventional photo-reactors require the catalysts to be separated and recycled: typical catalytic particles (*e.g.*, TiO_2) have average size of 100 nm, so they are smaller than most commercial polymer filter papers (pore size: 0.1–0.45 μm). As a result, catalysts are difficult to remove from the final products and expensive post-processes are required after water treatment. Furthermore, their large surface area-to-volume ratio and surface energy create a strong tendency for catalyst agglomeration during operation.

A technology based on MPR, where the catalyst is immobilized on the surface or on the pores of the membrane *e.g.* fixed catalyst approach,[3] would remove the need for post-treatment processes, allowing for low energy consumption, automatic control, continuous operation with simultaneous catalyst and product separation. Other advantages include low maintenance and strong flexibility, as more complex reactors can be built by connecting more membranes into modules.[46] However, the lack of control of catalyst load and distribution in the membrane strongly reduces the photo-catalytically active surface and causes the photo-conversion kinetics to strongly depend on the mass-transfer processes of the dyes from the liquid to the catalyst surface.[46] Overall, this strongly reduces the MPR photo-catalytic efficiency, when compared to traditional photo-reactors. This explains why MPR typically requires very thick catalytic beds (even up to 1 m)[46] and a very long water treatment process (up to hours).[47] Furthermore, the membrane structure and material properties are also important in determining if and how the dyes can interact with the catalyst. Ideally, the membrane should enhance surface contact with the dyes and should not deteriorate over the reaction time. Therefore, the discovery of new materials is fundamental in developing novel and efficient MPRs.

Previous works[25,48–51] have used 2D-crystals to support catalytic nanoparticles; however, the catalysts are weakly bonded to the 2D crystals, so they detach from the support, resulting in reduced photo-activity over the reaction time.

One has to remember that 2D crystals show unique properties not only when used as individual nanosheets, but also when assembled into membranes. Laminates composed by millions of nanosheets all stacked to each other show very different properties compared to the corresponding bulk material.[52,53] For example, membranes made of graphene oxide nanosheets have shown unique properties, such as selective permeation of water, opening the possibility of using these membranes for gas or liquid separation.[54–57]

Here, we demonstrate the use of the g-C_3N_4 laminate as a self-catalytic MPR: in this approach, the membrane is the catalyst itself, so separation and chemical reaction happen *in situ* and at the same time. Nanosheet-based membranes can be easily fabricated by vacuum filtration.[58,59] Because the catalytic activity strongly depends on the precise structure (defects, amount of edges exposed, *etc.*) characterization of the membranes was performed using several techniques.[60] Fig. 2A shows that the X-Ray Diffraction (XRD) characteristic of the molecular precursor (melamine) disappears in either the g-C_3N_4 bulk or membrane. Therefore, we can exclude any melamine residuals or derivatives in either the bulk or nanosheet g-C_3N_4. The XRD spectrum of g-C_3N_4 bulk and nanosheet-based membrane is characterized by a strong peak at 27.8°, the typical interlayer stacking (002) peak of graphite, corresponding to a distance of 0.326 nm.[61] In bulk g-C_3N_4 a small peak at 13° is visible, corresponding to an in plane structural packing motif, due to the tri-*s*-triazine patterning.[17,32] Note that the in-plane repeat period observed (0.681 nm) is smaller than the one of

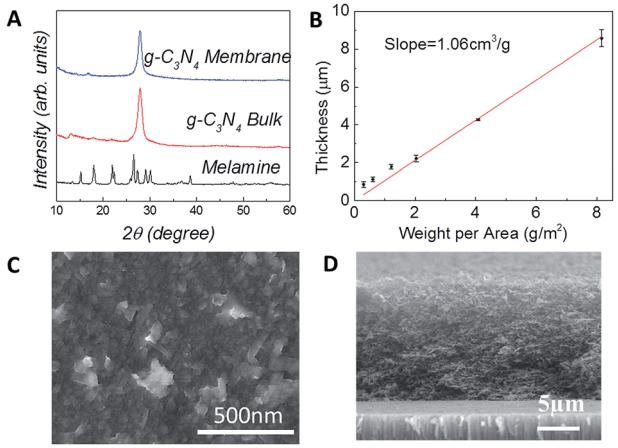

Fig. 2 (A) X-ray diffraction pattern of melamine, g-C_3N_4 bulk and membrane; (B) thickness of g-C_3N_4 laminates as a function of the weight per area; in-plane (C) and cross section (D) SEM images of a g-C_3N_4 membrane.

tri-*s*-triazine (~0.713 nm) and this has been attributed to small tilt angularity in the structure.[17] In g-C_3N_4 nanosheets this peak seems to shift at ~16°, indicating an increase in tilting. This is expected considering that nanosheets usually assemble with tilting angles in the laminate, giving rise to a structure with pores and capillaries (see Fig. 1 in ref. 62). Note that the XRD of our membrane is very different from measured powder obtained after drying the g-C_3N_4 dispersion at 60 °C in vacuum.[40] In this case a loose and irregular morphology was obtained, while in our work a more ordered and graphitic morphology, still retaining the inter-planar tri-*s*-triazine characteristics of the initial material, has been observed. We measured the thickness of the laminate by scanning electron microscopy (SEM). As shown in Fig. 2B, the thickness of the laminate is found to be proportional to the weight per area. The slope is 1.06 ± 0.04 cm^3 g^{-1}, so the density of the laminate is ~0.94 g cm^{-3}, which is smaller than the density of a g-C_3N_4 crystal (2.5 g cm^{-3}).[63] Fig. 2C and D show in plane and cross-section SEM images of the laminate, respectively, confirming that the membrane is composed by partially overlapped and tilted nanosheets, giving rise to a characteristic porous structure. This is confirmed by transmission electron microscopy (TEM) (Fig. S5†). The characteristic structure of the g-C_3N_4 membrane allows water to flow between the layers and at the same time maximizes the number of catalytic active sites at the solution–catalyst interface, Fig. 3A.

We tested this idea by evaluating the residual dye content by UV-Vis spectroscopy after the liquid has flown through the membrane. In a typical process, 1 mg of g-C_3N_4 nanosheets is deposited on an alumina oxide filter with pore size of 0.02 μm (Whatman Inc.) by vacuum filtration. Then, the water containing 5×10^{-5} M of dye was pumped through the membrane with a flow rate of 2 mL h^{-1} under irradiation with a lamp. To demonstrate the versatility of this method, we studied the photo-degradation of three dyes often used in the textile industry: Sudan orange G (SG), Rhodamine 110 (Rh) and Methylene Blue (MB). We found that less than 1% of the dye was left in the collected water after flowing through the g-C_3N_4 laminate, Fig. 3B, showing that this approach has comparable efficiency to the process based on individual nanosheets (see ESI†). Furthermore, we tracked the reaction over time to investigate the stability of the process. The time-dependent flux conversion efficiency [FE(t)] is given by: $\mathrm{FE}(t) = 1 - C_f(t)/C_0$, where C_f refers to the concentration of the dyes left in the treated liquid at a certain time, and C_0 is the starting dye content. Fig. 3C shows that g-C_3N_4 membranes achieve a FE of ~100% for several hours.

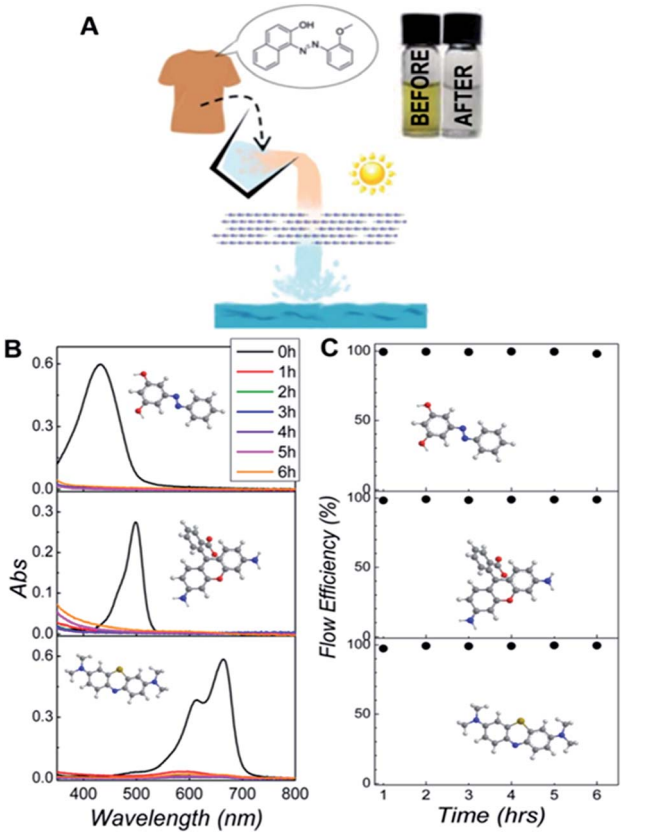

Fig. 3 (A) Schematic of the MPR used for degradation of Sudan orange G (SG) and pictures of the dispersions before and after treatment. (B) Time-evolution of the UV-Vis spectra for all three dyes investigated: Sudan orange G (SG), Rhodamine 110 (Rh) and methylene blue (MB). (C) Flow efficiency measured over 6 hours for different organic pollutants.

In order to confirm that the decrease in concentration is neither due to simple adsorption on the surface of the membrane[1] nor the rejection by the interlayer spacing, we also performed a control experiment, where the same amount of solution has been filtered under dark conditions. We found that only ~5.4% of SG gets physisorbed in a ~2 μm thick laminate (Fig. 4). Therefore, this shows that most of the molecules can move through the nanosheets and that changes in the dye concentration are mainly produced by photo-degradation. In the case of positively charged Rh and MB, the effect of the physical absorption increases to ~20%, probably due to steric effects with negatively charged g-C_3N_4. Two very recent references indicate that g-C_3N_4 incorporated with graphene oxide[64] or polymer[65] can act as a separation membrane. However, the

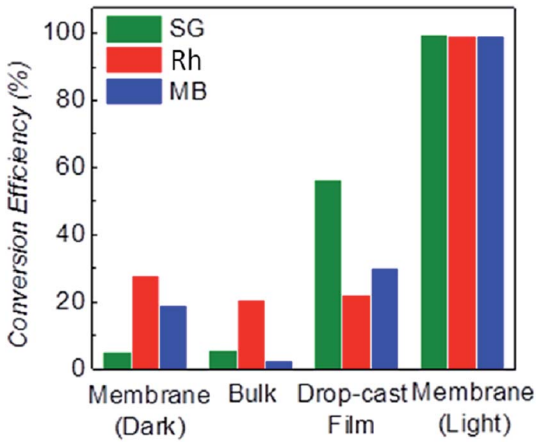

Fig. 4 Conversion efficiency measured after 2 h using three different types of g-C_3N_4 (bulk g-C_3N_4, drop casted g-C_3N_4 film and g-C_3N_4 laminates obtained by filtration). A control experiment in the dark was also performed for the g-C_3N_4 laminates to evaluate the adsorption ability of the membrane.

bare g-C_3N_4 membrane is unable to separate organic dyes from water under dark conditions. Therefore, the separation function of the membrane is not the dominant effect for the degradation.

The experiment shown in Fig. 3A was also performed by replacing the laminate with g-C_3N_4 bulk (Section 3.2.2 in ESI†). We observed that only 5.8% of SG was degraded by the bulk g-C_3N_4 (Fig. 4), confirming the higher degradation efficiency of the g-C_3N_4 laminate. Note that laminates produced by simple drop-casting show reduced degradation efficiency, due to the non-uniform laminate surface and to the tiny cracks produced from the evaporation of the solvent, Fig. S15.† However, we believe an improved solution processed coating method may result in better degradation performance, for instance, the HNO_3 assisted coating method as reported by Wang *et al.* recently.[66]

The superior degradation efficiency of the g-C_3N_4 nanosheet-based membranes is attributed to the increased amount of catalyst active sites available to the dye, when the mobile phase is traveling in the membrane (Fig. 5A). This is confirmed by studying the conversion efficiency for membranes of increasing thickness from ~0.8 to ~2 μm: the thicker the membrane, the higher the conversion rate (Fig. 5B). Furthermore, there is an additional effect that could be responsible for the superior efficiency: the reaction is expected to happen in the small interlayer space between the nanosheets (~1 nm). It is known that confinement in nanopores and nanobubbles can strongly affect nucleation of organic crystals and chemical reactions,[67–69] so the interlayer space may act as a nanoreactor for the photochemical degradation of the dye, improving the kinetic rate.

As a consequence, the whole laminate can be treated as a series connection of numerous nanoreactors. Using the model of series reactor, we can further understand the high efficiency of the g-C_3N_4 laminate. Under this approach, a large number of small volume reactors in series is characterized by higher conversion efficiency than few large volume reactors in series (ESI†).

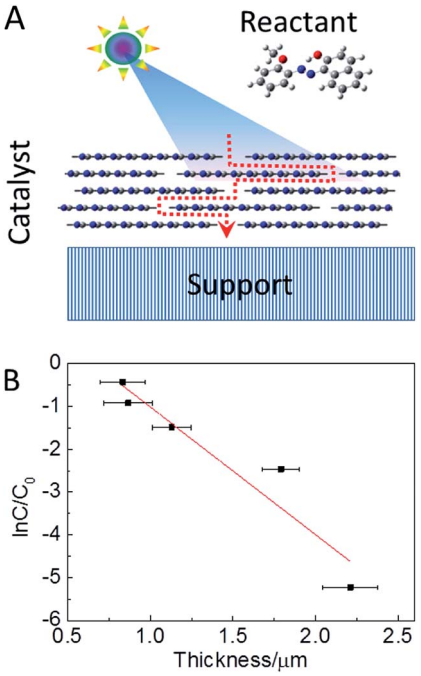

Fig. 5 (A) Schematic of 2D-nanosheets based reactor for photo-degradation. (B) Change in the concentration of SG after 2 h as a function of the laminate thickness.

Conclusions

In summary, we have demonstrated that g-C_3N_4 membranes can be used to make low-cost, efficient, easy-to-produce MPRs for water treatment under visible light. The high efficiency of this type of MPR is attributed to its structure and composition: the membrane is porous, allowing the water to move in the reactor; at the same time, the reactor is made of g-C_3N_4 nanosheets, which are efficient photo-catalysts for degradation of organic pollutants because their larger surface area. In this reactor, because the space between g-C_3N_4 nanosheets is comparable to the size of the dyes, the probability of the reactants to be close to the catalyst is enhanced, making the reaction very efficient. The membrane can be therefore considered a self-catalytic reactor. Since g-C_3N_4 has been shown to be an efficient photo-catalyst for many reactions under visible light, from water splitting to oxidization of alkanes and olefins, we expect self-catalytic MPRs to find several applications in sustainable chemistry.

Experimental methods

The preparation of g-C_3N_4 nanosheet

The yellow powder of graphitic carbon nitride (g-C_3N_4) bulk phase was prepared by a thermal annealing of melamine (Sigma Aldrich Inc.) at 600 °C for 1.5 hours.[70] 30 mg of g-C_3N_4 bulks was mixed with 10 mL isopropanol and water mixtures. The soya-like suspension was mild sonicated in a bath cleaner (DAWE 6290 A, 150 W, 25 kHz) for 12 hours to obtain the dispersion of g-C_3N_4 nanosheets. The large bulk was removed by

a centrifugation at 1000 rpm (~79 g) for 10 min. To further separate the thin layered g-C_3N_4, the supernatant (top 2/3) obtained in the last process was then centrifuged at 3000 rpm (~664 g) for 10 min. The top 1/2 supernatant of g-C_3N_4 was collected for the further characterizations. To avoid the signal overflow, 0.5 mL g-C_3N_4 dispersion was diluted ten times by the corresponding solvent mixture for the measurement of UV-Vis absorption (Cary 300, Varian Inc.).

The fabrication of the fixed-bed catalyst membrane

By using vacuum filtration, a dispersion containing 1 mg catalyst was deposited on the anodisc alumina oxide paper (0.02 μm pore size, 25 mm diameter, Whatsman Inc.). The laminate was characterized by X-ray diffraction (RINT2100; Rigaku, Japan) and scanning electron microscope (FEI XL30 ESEM-FEG). The error bar in Fig. 5 is calculated by analyzing 20 different SEM cross sections for each sample.

The photo-degradation

The photo-degradation was performed under a 100 W mercury lamp with a cutoff filter to remove the light below 400 nm. The flow efficiency of the catalytic degradation is calculated by following equation: flow efficiency $= (1 - C(t)/C(0))$, where $C(0)$ represents the starting concentration of the organic pollutant, $C(t)$ is the concentration of the pollutant at a certain time. Based on Lambert–Beer law, we can replace $C(t)$ by the absorbance measured at 433 nm for SG, at 499 nm for Rh and 664 nm for MB.

Acknowledgements

KGZ acknowledges the Royal Society in the framework of the Newton Fellowship scheme. This work was partially funded by the EPSRC Grants No. EP/K016946/1 (graphene-based membranes) and EP/K039547/1 and the ERC-Co grant (NOC2D).

Notes and references

1 V. K. Gupta, I. Ali, T. A. Saleh, A. Nayak and S. Agarwal, *RSC Adv.*, 2012, **2**, 6380–6388.
2 S. Karthikeyan, V. K. Gupta, R. Boopathy, A. Titus and G. Sekaran, *J. Mol. Liq.*, 2012, **173**, 153–163.
3 V. K. Gupta, S. K. Srivastava, D. Mohan and S. Sharma, *Waste Manage.*, 1998, **17**, 517–522.
4 A. L. Linsebigler, G. Lu and J. T. Yates, *Chem. Rev.*, 1995, **95**, 735–758.
5 C. Burda, Y. Lou, X. Chen, A. C. S. Samia, J. Stout and J. L. Gole, *Nano Lett.*, 2003, **3**, 1049–1051.
6 R. Asahi, T. Morikawa, T. Ohwaki, K. Aoki and Y. Taga, *Science*, 2001, **293**, 269–271.
7 H. Irie, Y. Watanabe and K. Hashimoto, *J. Phys. Chem. B*, 2003, **107**, 5483–5486.
8 X. Chen, L. Liu, P. Y. Yu and S. S. Mao, *Science*, 2011, **331**, 746–750.
9 H. Lin, L. Li, M. Zhao, X. Huang, X. Chen, G. Li and R. Yu, *J. Am. Chem. Soc.*, 2012, **134**, 8328–8331.
10 Y. Zhang, Z.-R. Tang, X. Fu and Y.-J. Xu, *ACS Nano*, 2011, **5**, 7426–7435.
11 Q. Xiang, J. Yu and M. Jaroniec, *J. Am. Chem. Soc.*, 2012, **134**, 6575–6578.
12 V. K. Gupta and T. A. Saleh, *Environ. Sci. Technol.*, 2013, **20**, 2828–2843.
13 V. K. Gupta, R. Kumar, A. Nayak, T. A. Saleh and M. A. Barakat, *Adv. Colloid Interface Sci.*, 2013, **193–194**, 24–34.
14 Y. Zheng, L. Lin, B. Wang and X. Wang, *Angew. Chem., Int. Ed.*, 2015, **54**, 12868–12884.
15 J. Zhang, Y. Chen and X. Wang, *Energy Environ. Sci.*, 2015, **8**, 3092–3108.
16 Y. Wang, X. Wang and M. Antonietti, *Angew. Chem., Int. Ed.*, 2012, **51**, 68–89.
17 X. Wang, K. Maeda, A. Thomas, K. Takanabe, G. Xin, J. M. Carlsson, K. Domen and M. Antonietti, *Nat. Mater.*, 2009, **8**, 76–80.
18 A. Thomas, A. Fischer, F. Goettmann, M. Antonietti, J.-O. Müller, R. Schlögl and J. M. Carlsson, *J. Mater. Chem.*, 2008, **18**, 4893–4908.
19 X. Wang, K. Maeda, X. Chen, K. Takanabe, K. Domen, Y. Hou, X. Fu and M. Antonietti, *J. Am. Chem. Soc.*, 2009, **131**, 1680–1681.
20 F. Goettmann, A. Thomas and M. Antonietti, *Angew. Chem., Int. Ed.*, 2007, **46**, 2717–2720.
21 F. Goettmann, A. Fischer, M. Antonietti and A. Thomas, *Angew. Chem., Int. Ed.*, 2006, **45**, 4467–4471.
22 J. Zhang, X. Chen, K. Takanabe, K. Maeda, K. Domen, J. D. Epping, X. Fu, M. Antonietti and X. Wang, *Angew. Chem., Int. Ed.*, 2010, **49**, 441–444.
23 X. Wang, S. Blechert and M. Antonietti, *ACS Catal.*, 2012, **2**, 1596–1606.
24 X. Chen, J. Zhang, X. Fu, M. Antonietti and X. Wang, *J. Am. Chem. Soc.*, 2009, **131**, 11658–11659.
25 X.-H. Li, J.-S. Chen, X. Wang, J. Sun and M. Antonietti, *J. Am. Chem. Soc.*, 2011, **133**, 8074–8077.
26 M. Shalom, S. Inal, C. Fettkenhauer, D. Neher and M. Antonietti, *J. Am. Chem. Soc.*, 2013, **135**, 7118–7121.
27 P. Zhang, Y. Wang, H. Li and M. Antonietti, *Green Chem.*, 2012, **14**, 1904–1908.
28 X.-H. Li, X. Wang and M. Antonietti, *ACS Catal.*, 2012, **2**, 2082–2086.
29 M. Zhang and X. Wang, *Energy Environ. Sci.*, 2014, **7**, 1902–1906.
30 M. Groenewolt and M. Antonietti, *Adv. Mater.*, 2005, **17**, 1789–1792.
31 Y. Wang, X. Wang, M. Antonietti and Y. Zhang, *ChemSusChem*, 2010, **3**, 435–439.
32 F. Goettmann, A. Fischer, M. Antonietti and A. Thomas, *Chem. Commun.*, 2006, 4530–4532, DOI: 10.1039/b608532f.
33 D. J. Martin, K. Qiu, S. A. Shevlin, A. D. Handoko, X. Chen, Z. Guo and J. Tang, *Angew. Chem., Int. Ed.*, 2014, **53**, 9240–9245.
34 J. Xu, L. Zhang, R. Shi and Y. Zhu, *J. Mater. Chem. A*, 2013, **1**, 14766–14772.
35 O. Abdulrahman, *Nanoscale*, 2013, **5**, 8921–8924.

36 X. Zhang, X. Xie, H. Wang, J. Zhang, B. Pan and Y. Xie, *J. Am. Chem. Soc.*, 2012, **135**, 18–21.
37 S. Yang, X. Feng, X. Wang and K. Müllen, *Angew. Chem., Int. Ed.*, 2011, **50**, 5339–5343.
38 M. J. Bojdys, N. Severin, J. P. Rabe, A. I. Cooper, A. Thomas and M. Antonietti, *Macromol. Rapid Commun.*, 2013, **34**, 850–854.
39 J. Tian, Q. Liu, A. M. Asiri, A. O. Al-Youbi and X. Sun, *Anal. Chem.*, 2013, **85**, 5595–5599.
40 Q. Lin, L. Li, S. Liang, M. Liu, J. Bi and L. Wu, *Appl. Catal., B*, 2015, **163**, 135–142.
41 S. Yang, Y. Gong, J. Zhang, L. Zhan, L. Ma, Z. Fang, R. Vajtai, X. Wang and P. M. Ajayan, *Adv. Mater.*, 2013, **25**, 2452–2456.
42 Y. Hernandez, V. Nicolosi, M. Lotya, F. M. Blighe, Z. Sun, S. De, I. T. McGovern, B. Holland, M. Byrne, Y. K. Gun'Ko, J. J. Boland, P. Niraj, G. Duesberg, S. Krishnamurthy, R. Goodhue, J. Hutchison, V. Scardaci, A. C. Ferrari and J. N. Coleman, *Nat. Nanotechnol.*, 2008, **3**, 563–568.
43 K.-G. Zhou, N.-N. Mao, H.-X. Wang, Y. Peng and H.-L. Zhang, *Angew. Chem., Int. Ed.*, 2012, **50**, 10839–10842.
44 U. Khan, A. O'Neill, M. Lotya, S. De and J. N. Coleman, *Small*, 2010, **6**, 864–871.
45 H. Zhao, H. Yu, X. Quan, S. Chen, H. Zhao and H. Wang, *RSC Adv.*, 2014, **4**, 624–628.
46 Y. Zhang, J. C. Crittenden, D. W. Hand and D. L. Perram, *Environ. Sci. Technol.*, 1994, **28**, 435–442.
47 G. Zayani, L. Bousselmi, F. Mhenni and A. Ghrabi, *Desalination*, 2009, **246**, 344–352.
48 S. Humaira, K. C. Kemp, C. Vimlesh and S. K. Kwang, *Nanotechnology*, 2012, **23**, 355705.
49 H. Zhang, P. Xu, G. Du, Z. Chen, K. Oh, D. Pan and Z. Jiao, *Nano Res.*, 2011, **4**, 274–283.
50 Y. Zhang, Z.-R. Tang, X. Fu and Y.-J. Xu, *ACS Nano*, 2010, **4**, 7303–7314.
51 H. Zhang, X. Lv, Y. Li, Y. Wang and J. Li, *ACS Nano*, 2009, **4**, 380–386.
52 R. R. Nair, M. Sepioni, I. L. Tsai, O. Lehtinen, J. Keinonen, A. V. Krasheninnikov, T. Thomson, A. K. Geim and I. V. Grigorieva, *Nat. Phys.*, 2012, **8**, 199–202.
53 R. R. Nair, I. L. Tsai, M. Sepioni, O. Lehtinen, J. Keinonen, A. V. Krasheninnikov, A. H. Castro Neto, M. I. Katsnelson, A. K. Geim and I. V. Grigorieva, *Nat. Commun.*, 2013, **4**, 2010.
54 R. K. Joshi, P. Carbone, F. C. Wang, V. G. Kravets, Y. Su, I. V. Grigorieva, H. A. Wu, A. K. Geim and R. R. Nair, *Science*, 2014, **343**, 752–754.
55 R. R. Nair, H. A. Wu, P. N. Jayaram, I. V. Grigorieva and A. K. Geim, *Science*, 2012, **335**, 442–444.
56 K. Huang, G. Liu, Y. Lou, Z. Dong, J. Shen and W. Jin, *Angew. Chem., Int. Ed.*, 2014, **53**, 6929–6932.
57 H. Li, Z. Song, X. Zhang, Y. Huang, S. Li, Y. Mao, H. J. Ploehn, Y. Bao and M. Yu, *Science*, 2013, **342**, 95–98.
58 G. Eda, G. Fanchini and M. Chhowalla, *Nat. Nanotechnol.*, 2008, **3**, 270–274.
59 D. A. Dikin, S. Stankovich, E. J. Zimney, R. D. Piner, G. H. B. Dommett, G. Evmenenko, S. T. Nguyen and R. S. Ruoff, *Nature*, 2007, **448**, 457–460.
60 T. A. Saleh and V. K. Gupta, *J. Colloid Interface Sci.*, 2012, **371**, 101–106.
61 Y. Zhang, Q. Pan, G. Chai, M. Liang, G. Dong, Q. Zhang and J. Qiu, *Sci. Rep.*, 2013, **3**, 1943.
62 F. Withers, H. Yang, L. Britnell, A. P. Rooney, E. Lewis, A. Felten, C. R. Woods, V. Sanchez Romaguera, T. Georgiou, A. Eckmann, Y. J. Kim, S. G. Yeates, S. J. Haigh, A. K. Geim, K. S. Novoselov and C. Casiraghi, *Nano Lett.*, 2014, **14**, 3987–3992.
63 J. Sehnert, K. Baerwinkel and J. Senker, *J. Phys. Chem. B*, 2007, **111**, 10671–10680.
64 Y. Wang, R. Ou, H. Wang and T. Xu, *J. Membr. Sci.*, 2015, **475**, 281–289.
65 K. Cao, Z. Jiang, X. Zhang, Y. Zhang, J. Zhao, R. Xing, S. Yang, C. Gao and F. Pan, *J. Membr. Sci.*, 2015, **490**, 72–83.
66 J. Zhang, M. Zhang, L. Lin and X. Wang, *Angew. Chem.*, 2015, **127**, 6395–6399.
67 J.-M. Ha, J. H. Wolf, M. A. Hillmyer and M. D. Ward, *J. Am. Chem. Soc.*, 2004, **126**, 3382–3383.
68 Y. Diao, T. Harada, A. S. Myerson, T. Alan Hatton and B. L. Trout, *Nat. Mater.*, 2011, **10**, 867–871.
69 C. H. Y. Xuan Lim, A. Sorkin, Q. Bao, A. Li, K. Zhang, M. Nesladek and K. P. Loh, *Nat. Commun.*, 2013, **4**, 1556.
70 S. C. Yan, Z. S. Li and Z. G. Zou, *Langmuir*, 2009, **25**, 10397–10401.